Korean J. Chem. Eng., **31**(3), 419-426 (2014)
DOI: 10.1007/s11814-013-0226-1

pISSN: 0256-1115
eISSN: 1975-7220

Kinetic modeling of hydrocracking reaction in a trickle-bed reactor with Pt/Y-zeolite catalysts

BalSang Lee*, Myung-June Park*,,†, Young-A Kim**, Eun Duck Park*,**, Jeongsik Han***, Kwang-Eun Jeong****, Chul-Ung Kim****, and Soon-Yong Jeong******

*Department of Chemical Engineering, Ajou University, Suwon 443-749, Korea
**Department of Energy Systems Research, Ajou University, Suwon 443-749, Korea
***Agency for Defense Development, Daejeon 305-152, Korea
****Green Chemistry Research Division, Korea Research Institute of Chemical Technology (KRICT), Daejeon 305-600, Korea
(*Received 7 May 2013 • accepted 26 October 2013*)

Abstract−A kinetic model is developed to predict the entire distribution of hydrocarbon products for the hydrocracking reaction with Pt/Y-zeolite catalysts in a trickle-bed reactor. Operating conditions, such as temperature, pressure, and wax and H_2 flow rates were varied to evaluate their effects on conversion and distribution, and kinetic parameters were estimated using the experimental data that covers the window of operating conditions. The comparison between experimental data and simulated results corroborated the validity of the developed model, and the quantitative prediction of the reactor performance was clearly demonstrated. To make evident the usefulness of the model, an optimization method, genetic algorithm (GA), was applied, and the optimal condition for the maximum production of C_{10}-C_{17} was successfully calculated.

Keywords: Hydrocracking, Pt/Y-zeolite Catalyst, Kinetic Modeling, Parameter Estimation, Optimization

INTRODUCTION

Synthetic fuels produced by the Fischer-Tropsch synthesis (FTS) have received increased attention as an alternative to fossil fuels due to their low content of sulfur, nitrogen, aromatics and heavy metals [1,2]. However, FTS products usually include a high fraction of long-chain normal paraffins, and thus, upgrade processes are required for their application as transportation fuels [3].

Hydrocracking is the process in which hydrogen is added to high boiling point fractions in order to produce middle distillates with low boiling points [4] by using bifunctional catalysts with metallic and acidic functions [5]. Operating conditions that are highly selective for quality middle distillates can range from 30 to 50 bar and 300 to 350 °C for pressure and temperature, respectively.

Kinetic modeling for hydrocracking has been intensively studied, mostly on the basis of lumped models owing to highly correlated elementary reactions between complex compounds [6-11]. Qader and Hill [11] conducted a kinetic study using a two-lump kinetic model (gas oil and their products) in a continuous fixed-bed reactor to analyze the kinetics of gas oil, and Callejas and Martinez [6] used a three-lump kinetic model (atmospheric residuum, light oils, gases) in an autoclave-stirred tank reactor. Moghadassi et al. [9] suggested a four-lump kinetic model (feed, diesel, gasoline, gases) in a fixed-bed reactor, and Martinez and Ancheyta [8] carried out the modeling of a continuously stirred tank reactor using a five-lump kinetic model (vacuum residue, vacuum gas oil, middle distillates, naphtha, gases). These lumped kinetic models have drawbacks in the sense that they provide averaged values of physical properties for a limited number of classes of products, and thus, the modeling approach at the mechanistic level for the entire chain length distribution has been introduced [7]. However, due to the large number of elementary steps involved in the hydrocracking reaction, a detailed mechanistic model is hardly applicable to complex mixtures, and the high computation load of the complicated model prohibits its use for optimization. Recently, the "all component" version of the hydrocracking model has been introduced, in which a division is established between linear and branched products, the latter being considered as a unique lump [10]. Although the mechanism has been simplified, the model effectively adheres to the chemicophysical nature of the system.

Our aim was to develop a kinetic model inclusive of the entire distribution of hydrocarbon products. As illustrated in our approach, chain lengths in the range of 10 to 17 carbons draw most of our focus since these are assumed to be the main components of jet fuels, although detailed criteria for jet fuels are based on several properties such as boiling points, density, viscosity, heat of combustion, thermal stability, etc. Experiments were conducted under a variety of conditions using Pt/Y-zeolite catalysts in a trickle-bed reactor, and the data were used to estimate kinetic parameters of the model. The developed model was then used to evaluate the effects of operating conditions and to determine the optimal operating conditions.

EXPERIMENTAL

Y-zeolite CBV series (Zeolyst International) was prepared and calcined at 500 °C for 4 h in air flow before impregnation. The tetraammineplatinum(II) nitrate precursor [$Pt(NH_3)_4(NO_3)_2$, Aldrich] was impregnated on CBV zeolite support with a fixed 1.0 wt% by

†To whom correspondence should be addressed.
E-mail: mjpark@ajou.ac.kr

incipient wetness impregnation (IWI) method. It was dried at 110 °C for 6 h followed by calcination at 500 °C for 4 h in air flow. The prepared catalyst was tested in a trickle-bed reactor with an outer diameter of 0.5 in. The catalyst (0.2 g) was diluted with inert alpha-alumina (0.8 g) to improve the temperature distribution along the catalytic zone. A tubular reactor with inner diameter of *ca* 1 cm (OD= 1/2in) was used, and the packing depth of the catalytic loading was 3.66 cm. Prior to activity testing, the catalyst was reduced at 500 °C for 2 h using 95 vol% H_2/Ar flow. The reaction conditions were 320-400 °C, 4.0-5.0 MPa, wax flow rate of 0.2-0.5 mL/min, and H_2 flow rate of 30-70 mL/min. The feed wax was a paraffinic Fischer-Tropsch (FT) wax (MP 329-331 K, Merck) whose chain length distribution is given in Fig. 1. The gaseous products were analyzed with a gas chromatograph (YL 6100, YL Instruments) equipped with a packed column (Carboxen (TM) 1000) for the thermal conductivity detector (TCD) and a capillary column (GS-GasPro, Agilent) for the flame ionization detector (FID). The liquid products were analyzed with a gas chromatograph (HP 5890, Hewlett Packard) equipped with a capillary column (BP-1) for the FID. The schematic diagram for the reaction apparatus is provided in Fig. 2.

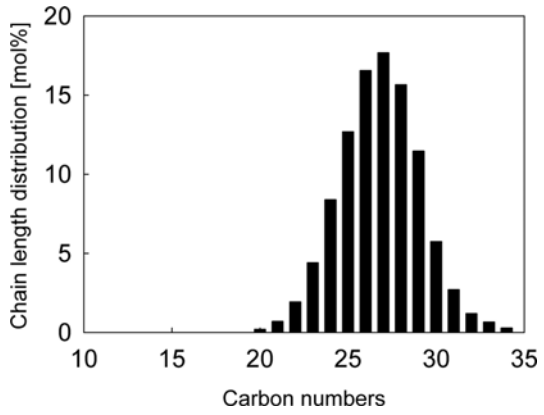

Fig. 1. Chain length distribution of the feed wax.

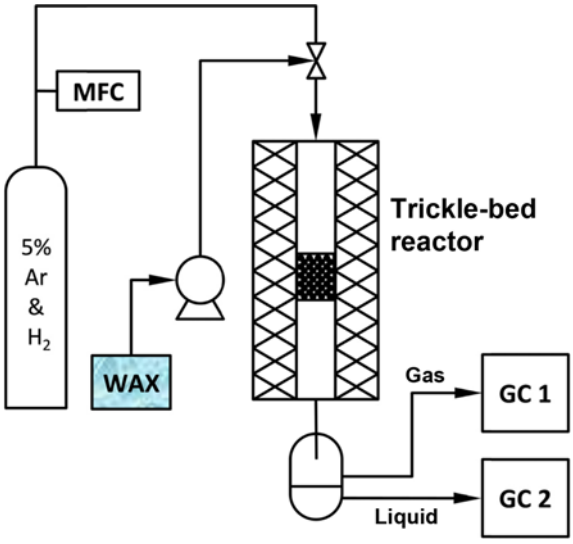

Fig. 2. Schematic diagram of the experimental system with a trickle-bed reactor.

RESULTS AND DISCUSSION

The overall reaction mechanism for the hydroisomerization and hydrocracking of linear paraffins is as follows: First, n-paraffins adsorb onto the catalytic surface, and then are dehydrogenated on the metal sites for the production of olefins, followed by their protonation on the acid sites to produce carbocations. After the rearrangement of carbocations, deprotonation or hydrocracking by β-scission takes place for the formation of iso-olefins or n/iso-paraffins, respectively [12]. However, since detailed elementary steps are too complicated for the development of reaction rates, Pellegrini et al. [13] simplified the steps as follows:

$$\text{n-C} \rightleftarrows \text{iso-C} \rightarrow \text{cracked products} \quad (1)$$

Here, all the types of isomers in the present study were assumed to be the isomer (iso-C) and olefins were also included in the iso-C because of the small amount observed in the experimental data. On the basis of the above mechanism, the reaction rates of isomerization (r_{iso}), cracking (r_{CR}), and the production of iso-C ($r_{prod,\,iso\text{-}C}$) and n-C ($r_{prod,\,n\text{-}C}$) by cracking are developed as follows (refer to Gamba et al. [14] for rate information):

$$r_{iso}(i) = A_{iso}(i)\exp\left(\frac{-E_{iso}(i)}{RT}\right)\left[fug_{n\text{-}C}(i) - \frac{fug_{iso\text{-}C}(i)}{K_{eq}(i)}\right] \Big/ ADS \quad (2)$$

$$r_{cr}(i) = A_{cr}(i)\exp\left(\frac{-E_{cr}(i)}{RT}\right) fug_{iso\text{-}C}(i) \Big/ ADS \quad (3)$$

$$r_{prod,iso\text{-}C}(i) = 2\gamma \sum_{m=6}^{C_{N,max}} P_{cr}(m,i)\, r_{cr}(m) \quad (4)$$

$$r_{prod,n\text{-}C}(i) = 2(1-\gamma) \sum_{m=6}^{C_{N,max}} P_{cr}(m,i)\, r_{cr}(m) \quad (5)$$

where ADS

$$= fug_{H_2}\left[1 + \sum_{i=1}^{C_{N,max}} K_{L,n\text{-}C}(i) fug_{n\text{-}C}(i) + \sum_{i=4}^{C_{N,max}} K_{L,iso\text{-}C}(i) fug_{iso\text{-}C}(i)\right] \quad (6)$$

The symbol i in parentheses denotes the length of chains, and γ is the fraction of isomers among cracked hydrocarbons. With respect to the physisorption of hydrocarbons, the Langmuir constant was assumed to be expressed as an exponential function of chain length on the basis of literature concerning adsorption in gas-solid systems [10], although the present study was conducted in a trickle-bed reactor (*cf.* the detailed correlation between K_L and i in Table 1). Maximum chain length (C_N^{max}) was specified as 34 since there were no chains longer than 34 in the feed wax (Fig. 1). Note that in some actual FTS processes, the maximum carbon number of hydrocarbon chain lengths shows higher than 34. However, the cracking process in the present study is considered to be applied to the FTS reaction system in our previous study [15], where most of hydrocarbon chain length ranged between 2 and 34, and thus, feed wax with chain length distribution in Fig. 1 is considered in the present study. In Eq. (4) and (5), $P_{cr}(m, i)$ represents the probability of iso-C(m) being converted to n/iso-C(i) by hydrocracking, and is defined as follows [14]:

$$P_{cr}(m,i) = \begin{cases} 1/(m-6) & i = 4, \cdots, (C_N^{max} - 4) \\ 1/2(m-6) & i = 3, (C_N^{max} - 3) \\ 0 & i = 1, 2, (C_N^{max} - 2), (C_N^{max} - 1), C_N^{max} \end{cases} \quad (7)$$

Table 1. Kinetic parameters used in the present study

Parameters	Units	Values		Remarks
		Frequency factor	Activation energy	
$k_{iso}(i)$	kmol/(kg_{cat}·h)	$(6.36\times10^{8})\ i^{6.52}$	$(3.08\times10^{4})\ \ln(i)+(1.70\times10^{4})$	Estimated
$k_{cr}(i)$	kmol/(kg_{cat}·h)	$(2.64\times10^{8})\ i^{7.13}$	$(8.62\times10^{3})\ \ln(i)+(9.72\times10^{4})$	
γ	-	0.82		
$K_{L,\,n\text{-}C}(i)$	Pa^{-1}	$293.96\exp\left[\frac{-\Delta H_{ads,n\text{-}C}(i)}{RT}\right]$		
$K_{L,\,iso\text{-}C}(i)$	Pa^{-1}	$191.91\exp\left[\frac{-\Delta H_{ads,iso\text{-}C}(i)}{RT}\right]$		
$K_{eq}(i)$	-	$0.19\times\exp(0.31\times(i))\left[\frac{-\Delta H_{iso}}{R}\left(\frac{1}{T}-\frac{1}{632.15}\right)\right]$		
$\frac{\Delta H_{ads,n\text{-}C}(i)}{R}$	kJ/kmol	$-(79.00+280.77i)$		[14]
$\frac{\Delta H_{ads,iso\text{-}C}(i)}{R}$	kJ/kmol	$-(0.03+261.97i)$		

This kinetic model is applied to a trickle-bed reactor, which is assumed to be an ideal plug flow reactor. Since the maximum chain length is 34, 66 mass balance equations (34 n-paraffins, 31 iso-paraffins and H_2) are defined as follows:

$$\frac{dF_{iso\text{-}C}(i)}{dW_{cat}} = -r_{iso}(i) + r_{prod,iso\text{-}C}(i) - r_{cr} \qquad i=6,\ldots,C_N^{max} \tag{8}$$

$$\frac{dF_{iso\text{-}C}(5)}{dW_{cat}} = -r_{iso}(5) + r_{prod,iso\text{-}C}(5) \tag{9}$$

$$\frac{dF_{iso\text{-}C}(4)}{dW_{cat}} = r_{prod,iso\text{-}C}(4) \tag{10}$$

$$\frac{dF_{n\text{-}C}(i)}{dW_{cat}} = r_{iso}(i) + r_{prod,n\text{-}C}(i) \qquad i=6,\ldots,C_N^{max} \tag{11}$$

$$\frac{dF_{n\text{-}C}(5)}{dW_{cat}} = r_{iso}(5) + r_{prod,n\text{-}C}(5) + \frac{2}{5}r_{cr}(6) \tag{12}$$

$$\frac{dF_{n\text{-}C}(i)}{dW_{cat}} = r_{prod,n\text{-}C}(i) + \frac{2}{5}r_{cr}(6) \qquad i=3,4 \tag{13}$$

$$\frac{dF_{n\text{-}C}(i)}{dW_{cat}} = \frac{2}{5}r_{cr}(6) \qquad i=1,2 \tag{14}$$

$$\frac{dF_{H_2}}{dW_{cat}} = \sum_{i=6}^{C_N^{max}} r_{cr}(i) \tag{15}$$

The kinetic model listed above provides a negative effect of the H_2/paraffin ratio since the fugacity of hydrogen (fug_{H_2}) is included in the denominator (Eq. (6)). This relationship contradicts the experimental data of the present study as well as results in other literature [16,17], although some reports claim a negative (or null) effect of the H_2/wax ratio in non-ideal hydrocracking conditions [18]. This discrepancy can be corrected by considering a vapor-liquid equilibrium (VLE) since complex mixtures under typical hydrocracking conditions exist in two different phases. When VLE occurs, an increase in H_2/wax ratio shifts the equilibrium toward the vapor phase, leading to the increase of hydrocarbon weight fractions in the vapor phase and the corresponding values of fugacity, as well as the decrease of the hydrogen fugacity. As a result, the reaction rate tends to increase, explaining the positive effect of the H_2/feed ratio on conversion. We estimated the fugacity of each species in the reaction mixture using the Soave-Redlich-Kwong (SRK) cubic equation of state (EOS). Due to the computation load, flash calculations are carried at ten points uniformly distributed along the reactor axis to find fugacities and fugacity coefficients of all components for

Table 2. Experimental conditions

No.	Temperature [°C]	Pressure [bar]	Wax flow rate [mL/min]	H_2 flow rate [mL/min]	H_2/C [mol/mol]	WHSV [$g_{wax}/(g_{cat}$·h)]	GHSV [mL-$H_2/(g_{cat}$·h)]
1	**320**	40	0.3	50	0.13	13.03	3000
2	**340**	40	0.3	50	0.13	13.03	3000
3	**360**	40	0.3	50	0.13	13.03	3000
4	**380**	40	0.3	50	0.13	13.03	3000
5	**400**	40	0.3	50	0.13	13.03	3000
6	360	**50**	0.3	50	0.13	13.03	3000
7	360	40	**0.2**	50	0.2	8.68	3000
8	360	40	**0.5**	50	0.08	21.71	3000
9	360	40	0.3	**30**	0.08	13.03	1800
10	360	40	0.3	**70**	0.18	13.03	4200

both liquid and vapor phases. Details about the vapor-liquid equilibrium (VLE) calculation procedure on the basis of SRK EOS are available in the literature [19,20]. Since the changes of temperature and pressure along the reactor axis are negligible and the vapor-liquid equilibrium between these calculation points is assumed to remain constant, ordinary differential equations (Eqs. (8)-(15)) are numerically solved with constant reaction rates for this interval. Since more frequent update of VLE calculation than ten points little influences the simulation results, the number of intervals is used as suggested in the literature [16].

To estimate kinetic parameters, experiments were conducted under ten controlled conditions (*cf.* conditions in Table 2), and wax conversions and entire distributions were measured in the units of % and C-mol% (mol% multiplied by carbon number), respectively. Since there was a significant amount of noise in the measurements, the data were smoothed using the 5-point moving average method (The simplest form of smoothing which simply replaces each data

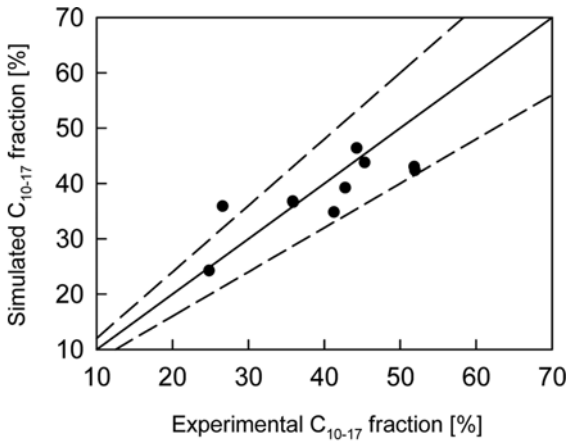

Fig. 3. Parity plot for the fraction of hycrocarbons with chain lengths between 10 and 17. Dashed lines correspond to 20% deviations.

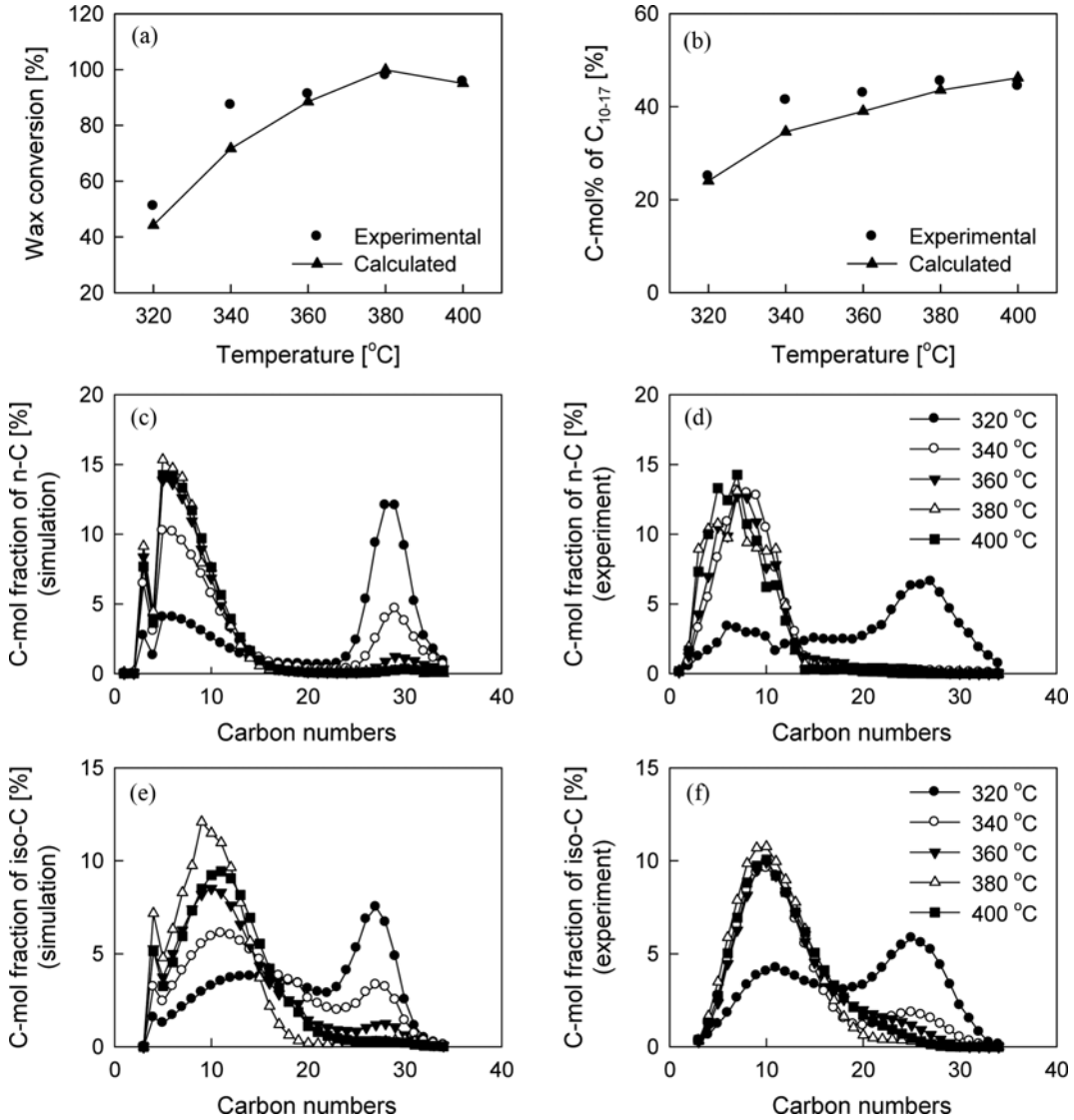

Fig. 4. (a) Wax conversion and (b) C-mol% of C(10-17) as a function of temperature (pressure=40 bar, wax flow rate=0.3 mL/min, H_2 flow rate=50 mL/min). Entire distribution of (c) simulated n-C, (d) experimental n-C, (e) simulated iso-C, and (f) experimental iso-C with varied temperature.

value with the average of neighboring values; to avoid shifting the data, it is best to average the same number of values before and after where the average is being calculated. See the reference [21] for more details). Parameters were estimated to fit experimental data by minimizing the objective function (Eq. (16)):

$$F_{obj}=\sum_{p}^{N_{eq}}\left[\sum_{q}^{NE} w_q\left(\frac{X_{q,calc}-X_{q,exp}}{X_{q,exp}}\right)^2\right]_p \quad (16)$$

where X_q represents the objective elements; wax conversion, C-mol% of n-C(k) (k=10, 15), C-mol% of iso-C(k) (k=10, 15), and isomer fraction were used in the present study. Since the aim of the present study is to exclusively produce jet fuels with chain lengths between 10 and 17, chain lengths of 10 and 15 were used for both n-C and iso-C. The subscripts "exp" and "calc" denote the experimental data and simulated results, respectively. The estimation was conducted using the *lsqcurvefit* function in MATLAB (MathWorks, Inc.), which applies the Levenberg-Marquardt algorithm for the optimization, and the estimated kinetic parameters are summarized in Table 1. The means of absolute relative residuals (MARR), defined as $100\sum|(y_{calc}-y_{exp})/y_{exp}|/N_{exp}$ are 11.8, 23.4, 27.3, 62.1, 15.23, and 13.2% for wax conversion, C-mol% of n-C(10), iso-C(10), n-C(15), iso-C(15), and isomer fraction, respectively, while the corresponding relative standard deviations (individual errors) are 18.8, 23.3, 36.9, 81.0, 17.8, and 3.28%. Note that relatively large values of mean of absolute relative residuals (MARR) are observed for some objective elements. This feature is attributable to the use of only two points (k=10, 15) as the objective elements, while all 34 chain lengths in the entire distribution are highly correlated with each other. Meanwhile, the sum of C-mol% of hydrocarbons with desired distributions, which is from C_{10} to C_{17}, shows good agreement between the calculated values and observed data, as shown in Fig. 3, and the values of MARR and relative standard deviations were 11.0% and 9.9%, respectively. In addition, comparing entire distributions between

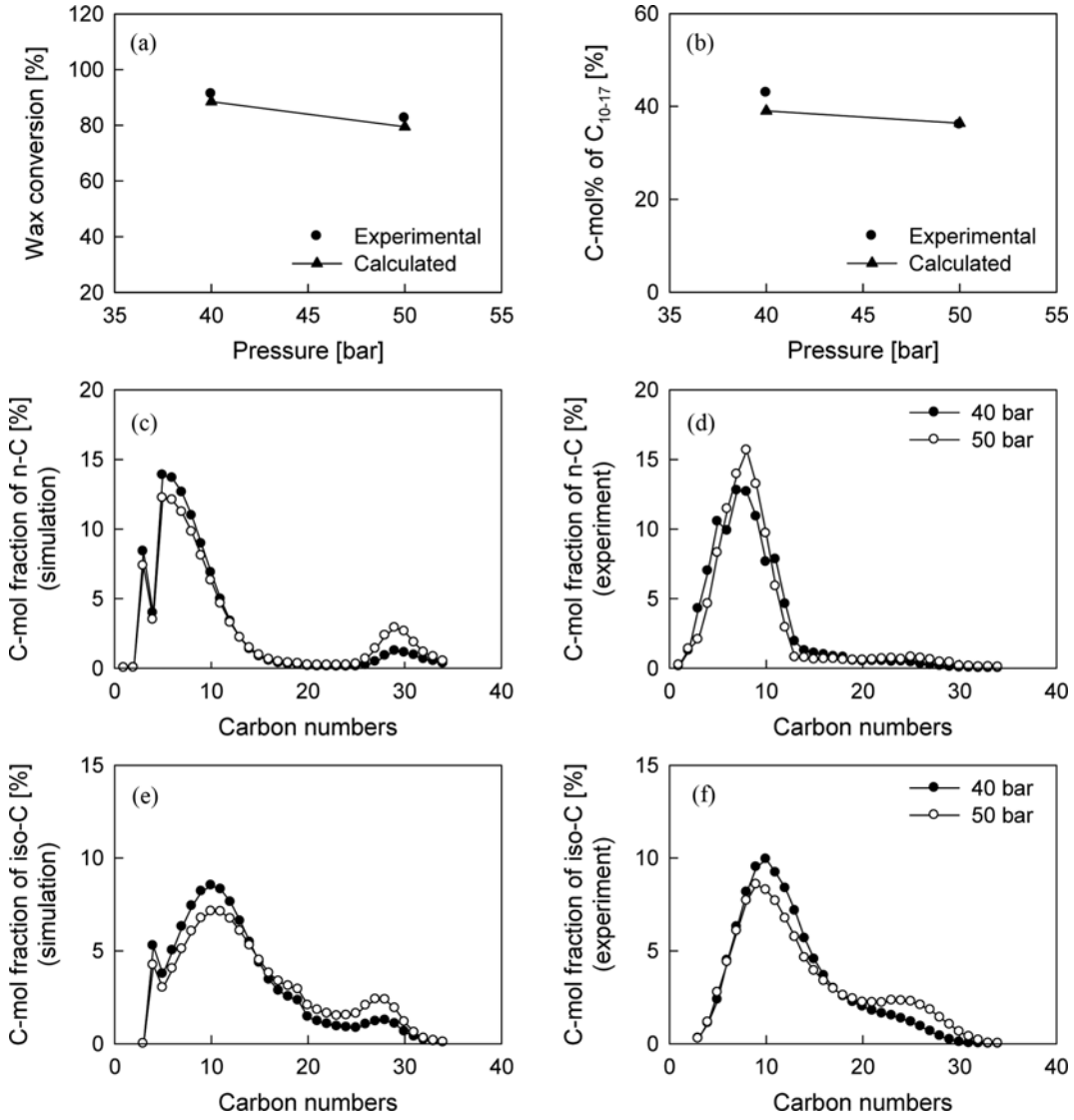

Fig. 5. (a) Wax conversion and (b) C-mol% of C(10-17) as a function of pressure (temperature=360 °C, wax flow rate=0.3 mL/min, H_2 flow rate=50 mL/min). Entire distribution of (c) simulated n-C, (d) experimental n-C, (e) simulated iso-C, and (f) experimental iso-C with varied pressure.

experimental data and simulated results also shows satisfactory performance of the model (*cf.* Figs. 4-7). Also, among estimated parameters, γ (fraction of isomers coming from the cracking of heavier hydrocarbons) plays a very important role in predicting the isomer fraction in the reactor effluent and may be dependent on experimental conditions. However, due to the limited number of experimental data, the value was assumed to be constant under all operating conditions. Despite the assumption, the averaged error of isomer fraction was comparable to the other objective elements in the present study, although the correlation equation between γ and experimental conditions might improve the performance of the model.

To examine the effects of operating conditions, conversion, C-mol% of C(10-17), and entire distributions of n-C and iso-C were drawn as a function of temperature, pressure, wax flow rate, and H_2 flow rate in Figs. 4 through 7. As shown in Fig. 4(a), wax conversion is increased with increasing temperature, but a small decrease is observed at the highest temperature, probably due to the vaporization of feed waxes. The amount of C(10-17) hydrocarbons also increases with temperature, and the effect of temperature on the entire distribution shows similar behavior with conversion (*cf.* Figs. 4(c) through 4(f), where Figs. 4(c) and 4(e) represent simulated results, while Figs. 4(d) and (f) are experimental data). In the case of n-C, simulation results (Fig. 4(c)) show the increase of peaks in low carbon number range (C5-C15) for the increase of temperature from 320 to 360 °C while no further increase is observed for higher temperature, and the corresponding peaks of iso-C (Fig. 4(e)) show gradual increase with increasing temperature. Meanwhile, experimental data of chain length distributions (Figs. 4(d) and 4(f)) show little effect of temperature, probably due to measurement errors.

Under the one condition with increased pressure, both the wax conversion and the fraction of C(10-17) are slightly decreased (Figs. 5(a) and 5(b)). Simulated distributions of n-C (Fig. 5(c)) and iso-C (Fig. 5(e)) also show small increase of peaks in low carbon number range (C5-C15), as are in experimental observations (Figs. 5(d)

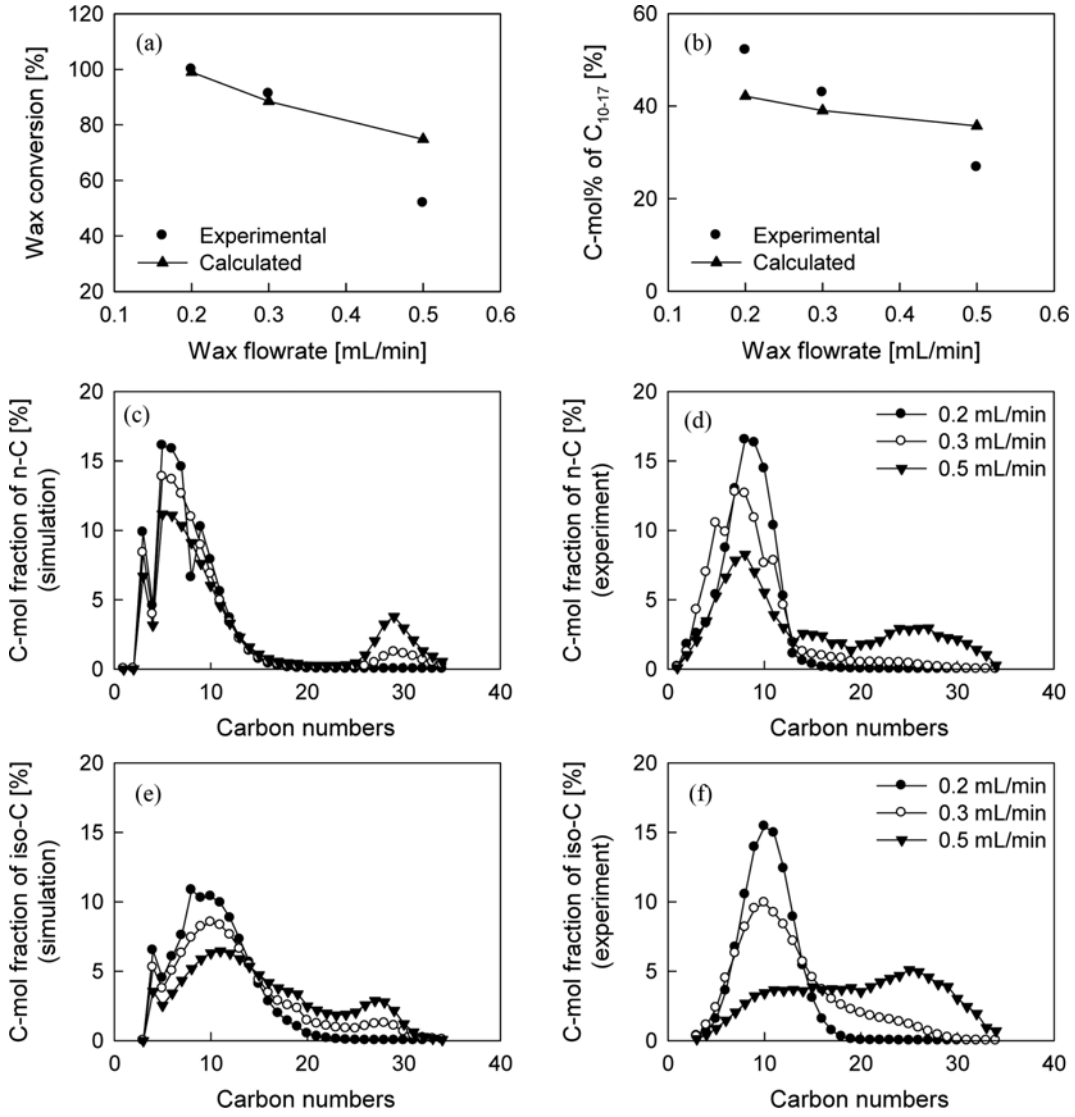

Fig. 6. (a) Wax conversion and (b) C-mol% of C(10-17) as a function of wax flow rate (temperature=360 °C, pressure=40 bar, H_2 flow rate=50 mL/min). Entire distribution of (c) simulated n-C, (d) experimental n-C, (e) simulated iso-C, and (f) experimental iso-C with varied wax flow rate.

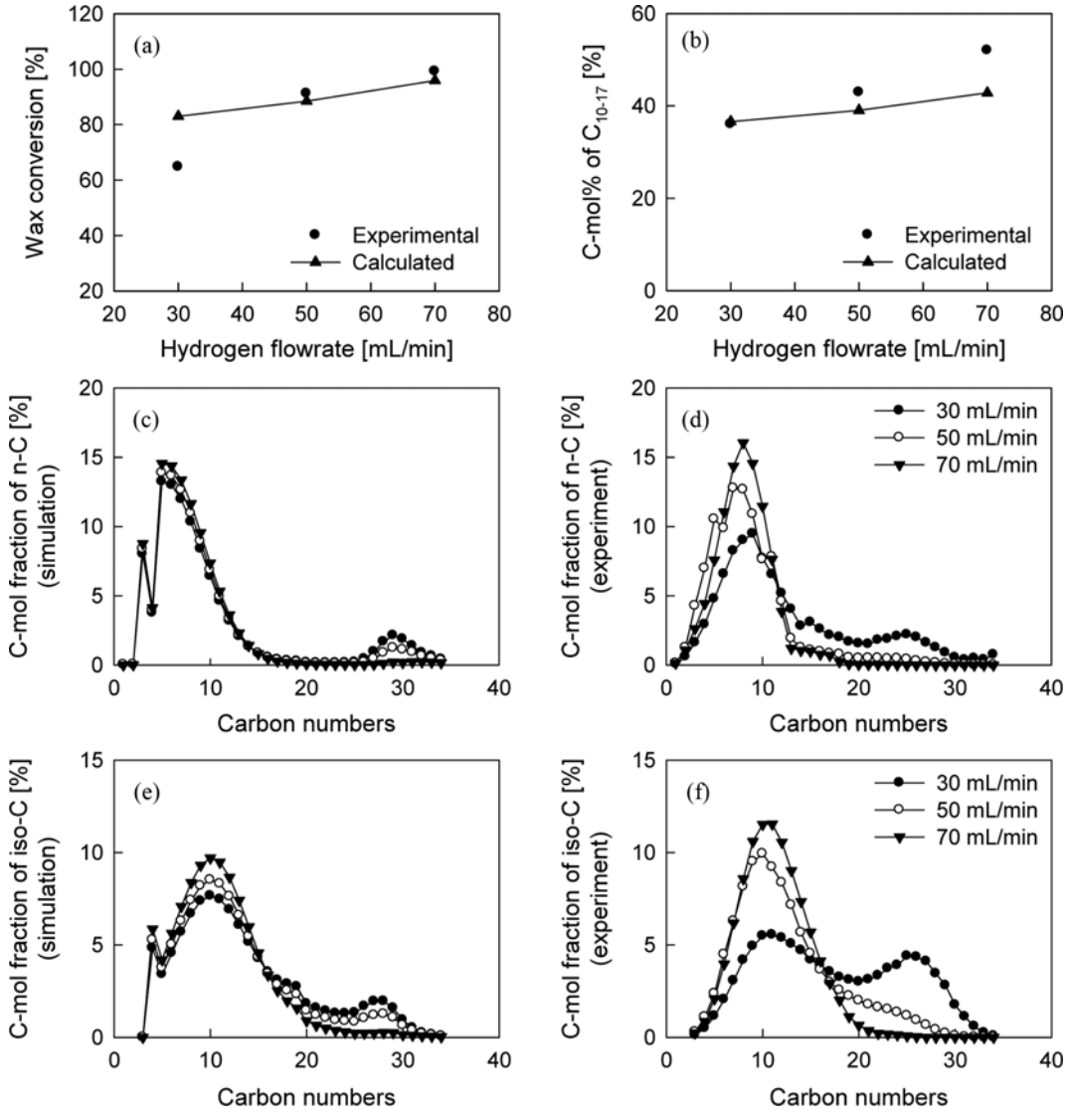

Fig. 7. (a) Wax conversion and (b) C-mol% of C(10-17) as a function of H_2 flow rate (temperature=360 °C, pressure=40 bar, wax flow rate=0.3 mL/min). Entire distribution of (c) simulated n-C, (d) experimental n-C, (e) simulated iso-C, and (f) experimental iso-C with varied H_2 flow rate.

and 5(f)). This result can be aptly explained by considering the reaction rates in Eqs. (2) through (6), where the order of the numerator is lower than that of the denominator. However, pressure may not have as significant an effect as temperature because the amount of liquid wax on the catalytic surface may not be affected much in the trickle-bed reactor.

When the wax flow rate is increased from 0.2 to 0.5 mL/min, wax conversion is decreased from 100% to 80% because of the increased amount of feed. Despite that, the productivity, which is the multiplication of the flow rate and the conversion, is increased. However, since high productivity with low conversion may require a great deal of separation capacity, the optimal flow rate should be considerately determined. In the case of wax flow rate change, both n-C and iso-C show gradual increase of peaks in low carbon number range (C5-C15) as a function of the flow rate, in simulations (Figs. 5(c) and 5(e)) as well as experiments (Figs. 5(d) and 5(f)).

Although the overall reaction mechanism in Eq. (1) does not account for the effect of hydrogen in the reaction, the reaction rates include the fugacity of hydrogen in the denominator, but the H_2/wax ratio was experimentally observed to have a proportionately positive effect. This feature was well accounted for in the model by applying the vapor-liquid equilibrium. The entire distribution also shows the increase of middle distillate with an increased H_2/wax ratio, but the degree of change in the simulation (Figs. 7(c) and 7(e)) is lower than that observed in the experimental data (Figs. 7(d) and 7(f)).

Finally, the benefit of the model was corroborated by determining the optimal operating variables. The genetic algorithm was applied to maximize the C(10-17) productivity with temperature, pressure, and wax and H_2 flow rates specified as arguments in the objective function. Input constraints were considered with the same operating windows in Table 2, except that the pressure ranged from 30 to 50 bar. The optimization was conducted using the genetic algorithm (GA) [22] to determine the optimal condition as 372.47 °C,

35.03 bar, wax flow rate of 0.49 mL/min, and H_2 flow rate of 55.19 mL/min, and the corresponding C(10-17) productivity was 13.16 mg/min, which is 2.48 times larger than the referenced case (the productivity of 5.29 mg/min with T=360 °C, P=40 bar, wax flow rate=0.3 mL/min and H_2 flow rate=50 mL/min). However, the optimized results show H_2/HC ratio of 112.6 mL/mL [=(55.19 mL/min)/(0.49 mL/min)], which is lower than the ratio of 166.6 mL/mL [=(50 mL/min)/(0.3 mL/min)] in the base case. In general, minimum required H_2/HC ratio is higher for processes under severe operating conditions such as higher feed flow rate and temperature, and constraints for the optimization should be re-specified for those processes.

CONCLUSIONS

For the hydrocracking reaction with Pt/Y-zeolite catalysts in a trickle-bed reactor, a kinetic model on the basis of a simplified mechanism was introduced, and kinetic parameters were estimated using experimental data with varying temperature, pressure, and wax and H_2 flow rates. The validity of the model was corroborated by the comparison of entire distribution between experimental data and simulated results. When vapor-liquid equilibrium was incorporated into the model, it could successfully predict the positive behavior of H_2/wax ratio, and the effects of operating conditions from the simulation study showed that temperature and flow rates can manipulate the distributions effectively. The benefit of the developed model was also illustrated by the optimization study, and thus, we concluded that the model in the present study can be used to design a more efficient reactor and to further optimize operating conditions for the hydrocracking process.

ACKNOWLEDGEMENTS

This work was supported by the Korea Institute of Energy Technology Evaluation and Planning (KETEP) under Energy Efficiency & Resources Programs (Project No. 2010201010008A) of the Ministry of Knowledge Economy, Republic of Korea.

NOMENCLATURE

A_i : frequency factor [kmol/(k_{gcat}·h)]
C_N^{max} : number of maximum chain length in the inlet waxes (=34 in the present study)
E_i : activation energy [kJ/kmol]
F : molar flow rate [kmol/h]
fug : fugacity [Pa]
K_L : Langmuir constant for physical adsorption [Pa^{-1}]
NE : number of objective elements
N_{exp} : number of experimental conditions
P_{cr} : cracking probability
R : gas constant [kJ/(kmol·K)]
r_i : reaction rate [kmol/(kg_{cat}·h)]
γ : fraction of isomers coming from the cracking of heavier hydrocarbons
W_{cat} : catalyst weight [kg]

REFERENCES

1. F. A. N. Fernandes and U. M. Teles, *Fuel Process. Technol.*, **88**, 207 (2007).
2. A. Y. Khodakov, W. Chu and P. Fongarland, *Chem. Rev.*, **107**, 1692 (2007).
3. J. P. Collins, J. J. H. M. Font Freide and B. Nay, *J. Nat. Gas Chem.*, **15**, 1 (2006).
4. I. Elizalde, M. A. Rodríguez and J. Ancheyta, *Appl. Catal. A: Gen.*, **382**, 205 (2010).
5. C. Bouchy, G. Hastoy, E. Guillon and J. A. Martens, *Oil Gas Sci. Technol.*, **64**, 91 (2009).
6. M. A. Callejas and M. T. Martínez, *Ind. Eng. Chem. Res.*, **38**, 3285 (1999).
7. M. T. Klein and G. Hou, *In practical advances in petroleum processing*, Ed. by C. S. Hsu, P. R. Robinson, Springer, New York, 187 (2006).
8. J. Martínez and J. Ancheyta, *Fuel*, **100**, 193 (2012).
9. A. R. Moghadassi, N. Amini, O. Fadavi and M. Bahmani, *Pet. Sci. Technol.*, **29**, 2416 (2011).
10. L. Pellegrini, S. Bonomi, S. Gamba, V. Calemma and D. Molinari, *Chem. Eng. Sci.*, **62**, 5013 (2007).
11. S. A. Qader and G. R. Hill, *Ind. Eng. Chem. Proc. Des. Dev.*, **8**, 98 (1969).
12. M. A. Baltanas, H. Vansina and G. F. Froment, *Ind. Eng. Chem. Prod. Res. Dev.*, **22**, 531 (1983).
13. L. Pellegrini, S. Locatelli, S. Rasella, S. Bonomi and V. Calemma, *Chem. Eng. Sci.*, **59**, 4781 (2004).
14. S. Gamba, L. A. Pellegrini, V. Calemma and C. Gambaro, *Ind. Eng. Chem. Res.*, **48**, 5656 (2009).
15. Y. H. Kim, D. Y. Hwang, S. H. Song, S. B. Lee, E. D. Park and M. J. Park, *Korean J. Chem. Eng.*, **26**, 1591 (2009).
16. C. Gambaro, V. Calemma, D. Molinari and J. Denayer, *AIChE J.*, **57**, 711 (2011).
17. D. Leckel, *Energy Fuels*, **19**, 1795 (2005).
18. J. W. Thybaut, C. S. Laxmi Narasimhan, J. F. Denayer, G. V. Baron, P. A. Jacobs, J. A. Martens and G. B. Marin, *Ind. Eng. Chem. Res.*, **44**, 5159 (2005).
19. Z. Nasri and H. Binous, *J. Chem. Eng. Jpn.*, **40**, 534 (2007).
20. H. S. Naji, *Emirates J. Eng. Res.*, **13**, 81 (2008).
21. A. Savitzky and M. J. E. Golay, *Anal. Chem.*, **36**, 1627 (1964).
22. M. R. Lee, M. J. Park, W. Jeon, J. W. Choi, Y. W. Suh and D. J. Suh, *Korean J. Chem. Eng.*, **28**, 2142 (2011).